energies

MDPI

Article

Comparative Study of Passivity, Model Predictive, and Passivity-Based Model Predictive Controllers in Uninterruptible Power Supply Applications

Shafquat Hussain [1], Abualkasim Bakeer [2], Ihab S. Mohamed [3], Mario Marchesoni [1,*] and Luis Vaccaro [1]

[1] Department of Electrical, Electronics and Telecommunication Engineering and Naval Architecture (DITEN), University of Genova, 16145 Genova, Italy; shafquat.hussain@edu.unige.it (S.H.); luis.vaccaro@unige.it (L.V.)
[2] Department of Electrical Engineering, Faculty of Engineering, Aswan University, Aswan 81542, Egypt; abualkasim.bakeer@aswu.edu.eg
[3] Luddy School of Informatics, Computing, and Engineering, Indiana University, Bloomington, IN 47408, USA; mohamedi@iu.edu
* Correspondence: mario.marchesoni@unige.it

Abstract: Voltage source converters are widely used in distributed generation (DG) and uninterruptible power supply (UPS) applications. This paper aims to find the controller that performs best when model changes occur in the system, showing insensitivity to parameter variations. A comparison of the finite control set model predictive controller (FCS-MPC), interconnection and damping assignment passivity-based controller (IDA-PBC), and passivity-based model predictive control (PB-MPC) reveals that the PB-MPC provides high resistance to these unexpected LC filter changes in the converter. The second aim of the paper is to reduce the total harmonic distortion (THD) of the output voltage of the three-phase voltage source inverter (VSI). A high total harmonic distortion (THD) value exists in the voltage waveform of the three-phase voltage source inverter (VSI), feeding a non-linear load. A MATLAB simulation was performed using three control techniques for a three-phase VSI feeding: linear load, unbalanced load, and non-linear load. The PB-MPC performs better than the FCS-MPC and IDA-PBC in terms of having a low THD value in the output voltage of the converter under all types of applied loads, improving the THD by up to 30%, and having low variation in THD with mismatched filter parameters, as shown in the bar charts in the results section. Overall, the PB-MPC controller improves the robustness under parameter mismatch and reduces the computational burden. PB-MPC reduces the THD value because it integrates power shaping and the injection of damping resistances into the VSI.

Keywords: interconnection and damping assignment passivity-based controlled (IDA-PBC); finite control set model predictive controller (FCS-MPC); passivity-based model predictive control (PB-MPC)

Citation: Hussain, S.; Bakeer, A.; Mohamed, I.S.; Marchesoni, M.; Vaccaro, L. Comparative Study of Passivity, Model Predictive, and Passivity-Based Model Predictive Controllers in Uninterruptible Power Supply Applications. *Energies* **2023**, *16*, 5594. https://doi.org/10.3390/en16155594

Academic Editor: Mojtaba Ahmadieh Khanesar

Received: 30 June 2023
Revised: 20 July 2023
Accepted: 21 July 2023
Published: 25 July 2023

1. Introduction

The voltage source inverter (VSI) plays a vital role in uninterruptible power supply (UPS) and distributed generation (DG) units. UPS is used to power loads, like personal computers, industrial automated equipment, and communication equipment. Controlled VSI is expected to have low harmonics [1], excellent ability to reject disturbances, and robustness to parameter mismatch [2].

In order to achieve the above-mentioned features in VSI, a simpler, linear, and more popular control approach was adopted, which utilizes a double-loop control in the inner current control loop and an outer voltage control loop PI controller [3,4]. While this PI controller is simple to implement and design, it has unsatisfactory performance during non-linear loading, and there exists a trade-off between the system's stability and transient response. To address these issues, several alternative controllers have been explored, including the proportional-resonant (PR) controller [5,6], feedback linearization [7], sliding

mode controller [8], repetitive controller [9], and Lyapunov-based controller [10]. These controllers have advantages and disadvantages in terms of dynamic performance, stability analysis, and system robustness.

Compared with linear control types, model predictive control employs different design methods. In the PI control technique, independent control loops are designed for every controlled variable, like voltage and current, before cascading them together. In the MPC control technique, the discrete model of the output filter is considered and the minimized cost function is evaluated at the predicted sampling time [11]. This cost function is based on the Euclidean distance between the controlled variable and its reference signal [12]. Other control objectives can be added easily because of their advantages, such as high robustness, good transient characteristics, non-linearities, and constraints. The FCS-MPC is an attractive method for controlling power electronic converters [13,14].

To stabilize the power system network and control the power electronic converters, there is a popular energy-based controller design approach, named interconnection and damping assignment passivity-based controlled (IDA-PBC). The circuit diagram of the IDA-PBC controller is shown in Figure 1. The controller takes feedback signals from the VSI and then converts them into a rotating frame (dq). This model is represented by a port-controlled Hamiltonian (PCH) model, and the controller can measure the natural energy of the system and find a state feedback control law. The IDA-PBC controller stabilizes the converter by making it dissipative or passive. The key advantage of using it is the guaranteed system stability, regardless of the complexity. It also offers satisfactory current tracking performance under non-linear loads [15]. The IDA-PBC controller has been deployed and analyzed in DC-DC converters, rectifiers, single-phase VSIs, three-phase PSIs, MMC converters, and DAB converters.

Sera [16] compared the performance of the IDA-PBC controller and the PI controller for the three-phase VSI. The parameter mismatch effect on the performance of the PBC control of the single-phase VSI has been studied and investigated by Komurcugil [17].

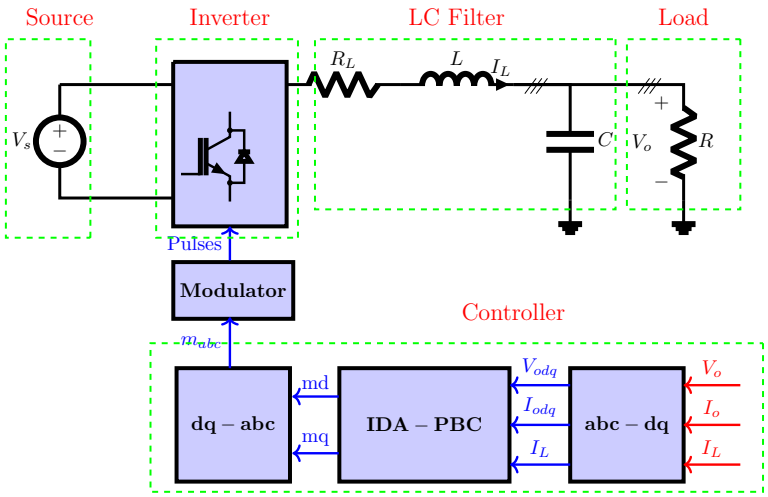

Figure 1. IDA-PBC controller for the three-phase voltage source inverter.

The passivity-based model predictive controller (PB-MPC) is formed by cascading passivity-based and MPC controllers. The reference signals are generated using a passivity-based controller, while the controlled objective is predicted and compared with the reference signals [18]. It provides a low THD value, which is robust to parameter mismatch. Moreover, it possesses high dynamic stability, there is no need for weighting factors, and it has low computational burden.

As shown in Table 1, various controllers for three-phase voltage source inverters have been discussed in the literature. The table highlights both the benefits and drawbacks of different control techniques for three-phase VSI. Table 1 shows that the PI controller performs poorly during non-linear and unbalanced loads, and the sliding mode controller

suffers from the chattering effect; using the gain scheduling method, the parameters are difficult to calculate, while the MPC controller bears a large computation burden. The IDA-PBC offers a promising tracking response to time-varying signals for switch mode power supplies (SMPS), rectifiers, single-phase inverters, and three-phase inverters. While PB-MPC provides low THD, and is robust to parameter mismatch compared to the other controllers, it also has other advantages compared to the FCS-MPC controllers, e.g., there is no need for weighting factors, high dynamic stability, and a comparatively lower computational burden.

Table 1. Literature on different control techniques of three-phase voltage source inverters.

Control Technique	Advantages	Disadvantages
Model's predictive control [19,20]	1. Free of mathematical modeling. 2. Maximum robustness 3. Rapid dynamic response and a settling time of 2.71 ms	1. Large computational burden 2. Much complexity in the algorithm
Gain Scheduling Method [21]	1. Contains a general model approach 2. Reduced cost 3. High robustness	1. Parameters are difficult to select
Sliding Model Control [2]	1. Simple implementation 2. Fast dynamic response 3. Robust to parameter variation and disturbance; settling time of 2.85 ms	1. Chattering effect problem
PI Control [22]	1. Easy to implement	1. High starting overshoot 2. Sensitive to controller gains 3. Sluggish response
IDA-PBC Control [23]	1. Stability ensures	
PB-MPC Controller [18]	1. Stability ensures 2. No weighting factors 3. Low computational complexity	Complex to design

Model predictive control, compared to a linear type of control, has different principles. In the PI control technique, independent control loops are designed for every controlled variable, like the voltage and current, before cascading them together. In the MPC control technique, the discrete model of the output filter is considered and the minimized cost function at the predicted sampling time is evaluated. That cost function (CF) is based on the Euclidean distance between the controlled variables, tracking the reference signal. Other control objectives can be easily added as a result of their advantages, like high robustness, good transient characteristics, non-linearities, and constraints. The FCS-MPC is an attractive way to perform the power electronic converter's control. This paper uses FCS-MPC to control the output voltage of a three-phase voltage source inverter (VSI), as shown in Figure 2.

This paper is organized as follows. In Section 2, IDA-PBC, FCS-MPC, and PB-MPC controllers are designed for the three-phase VSI. Section 3 presents the simulation results of the three-phase VSI using the IDA-PBC controller, FCS-MPC controller, and PB-MPC controller under different loading conditions, via a MATLAB simulation. In Section 4, our conclusions are shown.

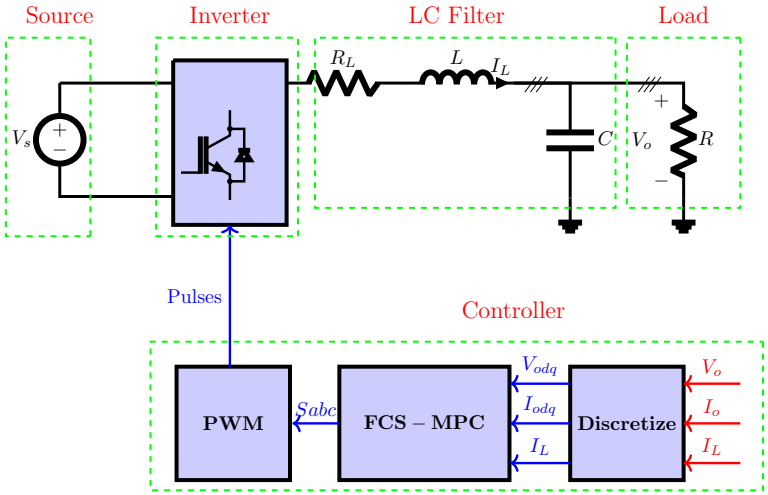

Figure 2. IDA-PBC controller for the three-phase voltage source inverter.

2. Design of Controllers

As discussed in the introduction, three-phase VSIs are widely used in uninterruptible power supply (UPS) applications and distributed generation systems (DGSs). The performance of the VSI depends on the controller's rise time, steady-state error, and dynamic performance. To design a fast dynamic response that provides better stability performance and reduces high THD values under linear, unbalanced, and non-linear loads, the IDA-PBC, FCS-MPC, and PB-MPC controllers were designed and validated for three-phase VSIs using a MATLAB simulation. The MATLAB simulation offers several advantages, including design simplicity, swift circuit design, high accuracy, functional integrity, and the reliability of results. Additionally, it enables easy and rapid control prototyping (RCP) for various DSPs and FPGAs.

2.1. IDA-PBC Controller Design

In the first part of the section, the IDA-PBC controller is designed and derived mathematically for the three-phase voltage source inverter (VSI) feeding a linear load with a dq reference frame. The port-controlled Hamiltonian (pH), the non-linear approach, is the IDA-PBC controller's base. The port-controlled Hamiltonian model contains an energy function called the Hamiltonian function, denoted by "H", which is used to define each energy-storing element, such as inductors and capacitors [23]. The port-controlled Hamiltonian model contains the physical structure of the three-phase inverter in terms of interconnections (J), damping (R), and energy storage functions (H) [24]. If the supplied energy to the system to be controlled is high and storing capability is low, then that system is said to be a passivity system. The port-controlled Hamiltonian system is represented by the following equation [16].

$$\frac{dx}{dt} = [J - R]\frac{\partial H(x)}{\partial x} + g(x)u + \zeta \tag{1}$$

where x denotes the state vector, J denotes the interconnection matrix, R denotes the damping matrix, $H(x)$ denotes the total energy stored in the system, $g(x)$ denotes the input matrix, ζ denotes the disturbances, u denotes the input control vector. The system, a standalone three-phase voltage source inverter (VSI), consists of a DC voltage source as a supply, and an H bridge inverter topology, with an LC filter at the output, as shown in Figure 1. The average model of the balanced three-phase system in the dq reference frame is expressed in the following equations [16]:

$$L\frac{di_{Ld}}{dt} = \frac{(m_d V_{dc})}{2} + \omega L i_{Lq} - r i_{Ld} - V_{od} \tag{2}$$

$$L\frac{di_{Lq}}{dt} = \frac{(m_q V_{dc})}{2} - \omega L i_{Ld} - r i_{Lq} - V_{oq} \tag{3}$$

$$C\frac{dV_{od}}{dt} = i_{Ld} - i_{od} + \omega C V_{oq} \tag{4}$$

$$C\frac{dV_{oq}}{dt} = i_{Lq} - i_{oq} - \omega C V_{od} \tag{5}$$

where L and C denote the inductance and capacitance values of the LC filter, and r denotes the effective series resistance of L. Equations (2) to (5) can be written in a port-controlled Hamiltonian form, as [16]:

$$\begin{bmatrix} L\frac{di_{Ld}}{dt} \\ L\frac{di_{Lq}}{dt} \\ C\frac{dV_{od}}{dt} \\ C\frac{dV_{oq}}{dt} \end{bmatrix} = \begin{bmatrix} -r & \omega L & -1 & 0 \\ -\omega L & -r & 0 & -1 \\ 1 & 0 & 0 & \omega C \\ 0 & 1 & -\omega C & 0 \end{bmatrix} \begin{bmatrix} i_{Ld} \\ i_{Lq} \\ V_{od} \\ V_{oq} \end{bmatrix} + \begin{bmatrix} \frac{V_{dc}}{2} & 0 \\ 0 & \frac{V_{dc}}{2} \\ 0 & 0 \\ 0 & 0 \end{bmatrix} \begin{bmatrix} m_d \\ m_q \end{bmatrix} + \begin{bmatrix} 0 \\ 0 \\ -i_{od} \\ -i_{oq} \end{bmatrix} \tag{6}$$

$$x = \begin{bmatrix} L i_{Ld} L i_{Lq} C V_{od} C V_{oq} \end{bmatrix}^T \tag{7}$$

$$J = \begin{bmatrix} -r & \omega L & -1 & 0 \\ -\omega L & -r & 0 & -1 \\ 1 & 0 & 0 & \omega C \\ 0 & 1 & -\omega C & 0 \end{bmatrix} \tag{8}$$

$$R = \begin{bmatrix} r & 0 & 0 & 0 \\ 0 & r & 0 & 0 \\ 1 & 0 & 0 & 0 \\ 0 & 1 & 0 & 0 \end{bmatrix} \tag{9}$$

$$H(x) = \frac{1}{2}\left(L i_{Ld}^2 + L i_{Lq}^2 + C V_{od}^2 + C V_{oq}^2 \right) \tag{10}$$

$$g(x) = \begin{bmatrix} \frac{V_{dc}}{2} & 0 & 0 & 0 \\ 0 & \frac{V_{dc}}{2} & 0 & 0 \end{bmatrix}^T \tag{11}$$

$$u = \begin{bmatrix} m_d m_q \end{bmatrix}^T \tag{12}$$

$$\zeta = \begin{bmatrix} 0 & 0 & -i_{od} & -i_{oq} \end{bmatrix}^T \tag{13}$$

V_{odq} and i_{odq} are the control variables that need to track their references with zero SSE. To achieve closed-loop stability and convergence, the term $H_d(x, x)$ should reach the minimum at the point of x. To achieve these requirements, as described in [16]:

$$0 = \frac{\partial H_d(x, x^*)}{\partial x} \tag{14}$$

$$\frac{\partial^2 H_d(x, x^*)}{\partial x^2} > 0 \tag{15}$$

$$\frac{dH_d(x,x^*)}{dt} = -\in^T P^{-1} R_d P^{-1} \in < 0 \tag{16}$$

R_d is the required damping resistance for the system to become stabilized; this method is known as the "Lyapunov direct method". To achieve stability, R_d should achieve the structure preservation condition, as described in [25]:

$$R_d = R + R_a = \begin{bmatrix} R & R_a \end{bmatrix}^T \tag{17}$$

where R_a is the dissipation matrix and contains the gains for the controller part. R_d is the positive semidefinite and Ra is the positive diagonal matrix, as described in [25].

$$R_a = \begin{bmatrix} R_1 & 0 & 0 & 0 \\ 0 & R_2 & 0 & 0 \\ 0 & 0 & R_3 & 0 \\ 0 & 0 & 0 & R_4 \end{bmatrix} \tag{18}$$

The desired interconnection matrix J_d should be anti-symmetric and satisfy the following conditions [25].

$$J_d = J + J_a = -\begin{bmatrix} J & J_a \end{bmatrix}^T \tag{19}$$

To decouple the dq-axis terms, the interconnection matrix J_a is chosen, according to [25]:

$$J_a = \begin{bmatrix} 0 & -\omega L & 0 & 0 \\ \omega L & 0 & 0 & 0 \\ 0 & 0 & 0 & -\omega C \\ 0 & 0 & \omega C & 0 \end{bmatrix} \tag{20}$$

The final equation, as outlined in [24], will be:

$$[J - R]\frac{\partial H_a(x,x^*)}{\partial \epsilon} + [J_a - R_a]\frac{\partial H_d(x,x^*)}{\partial \epsilon} - \zeta + \frac{dx^*}{dt} = g(x)u \tag{21}$$

By simultaneously solving the above equations, the reference current signals and modulating signals can be calculated as in [25]:

$$m_d = \frac{2}{V_{dc}}\left\{L\frac{di^*_{Ld}}{dt} + ri^*_{Ld} - \omega L i_{Lq} - R_1(i_{Ld} - i^*_{Ld}) + v^*_{od}\right\} \tag{22}$$

$$i^*_{Ld} = C\frac{dv^*_{od}}{dt} - R_3(v_{od} - v^*_{od}) + i_{od} - \omega C v_{oq} \tag{23}$$

$$m_q = \frac{2}{V_{dc}}\left\{L\frac{di^*_{Lq}}{dt} + ri^*_{Lq} + \omega L i_{Ld} - R_2\left(i_{Lq} - i^*_{Lq}\right) + v^*_{oq}\right\} \tag{24}$$

$$i^*_{Lq} = C\frac{dv^*_{oq}}{dt} - R_4\left(v_{oq} - v^*_{oq}\right) + i_{oq} + \omega C v_{od} \tag{25}$$

Equations (23) and (25) indicate the modulation indexes in the d and q axes, respectively, while Equations (24) and (25) generate the reference current. The implementation of the IDA-PBC controller relies on these four equations. By tuning the values R_1 through R_4, the VSI can perform satisfactorily.

2.2. FCS-MPC Design for Three-Phase VSI

In the second part of this section, the MPC controller is designed in MATLAB Simulink. The FCS-MPC relies on the model of the plant/system. To achieve good dynamic performance while implementing the FCS-MPC for VSC, both models for VSI and output filters

are required. The most commonly used topology of the VSI is the three-phase two-level VSI, as shown in Figure 3.

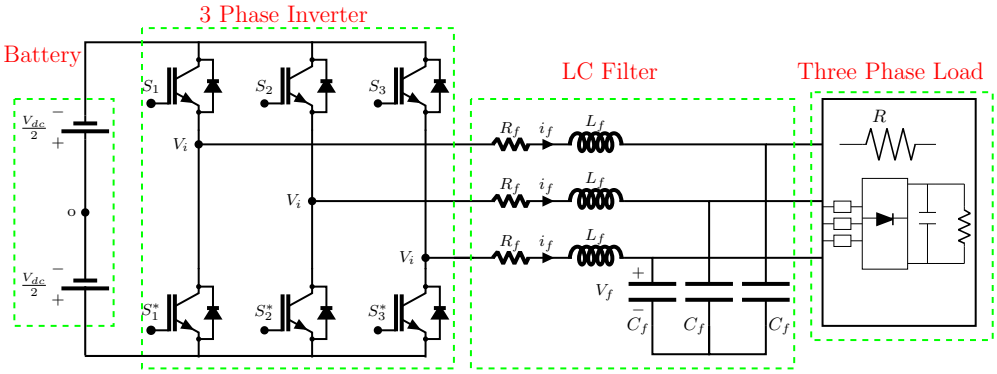

Figure 3. Three-phase Voltage source inverter with the LC filter.

As seen in Figure 3, the three-phase *LC* filter is connected to the output of a VSI. Each leg of a filter consists of an inductor (L_f), a series resistor (R_f), and a parallel connected capacitor with a capacitance of (C_f). The state variables are the current through the inductor and the voltage across the capacitor. The *LC* filter can be mathematically described as follows [26–28]:

$$L_f \frac{di_f}{dt} = V_i - V_f - R_f i_f \tag{26}$$

$$C_f \frac{dV_f}{dt} = i_f - i_o \tag{27}$$

$$\begin{bmatrix} i_f \\ V_f \end{bmatrix} = A * \begin{bmatrix} i_f \\ V_f \end{bmatrix} + B * \begin{bmatrix} V_i \\ i_o \end{bmatrix} \tag{28}$$

From Equation (28),

$$A = \begin{bmatrix} \frac{-R_f}{L_f} & \frac{-1}{L_f} \\ \frac{1}{C_f} & 0 \end{bmatrix} \tag{29}$$

$$B = \begin{bmatrix} \frac{1}{L_f} & 0 \\ 0 & \frac{-1}{C_f} \end{bmatrix} \tag{30}$$

The above equations denote the continuous state space model of an *LC* filter. The discrete model can be created using MATLAB with some particular discretization method, like the Tustin method, which has been used. The cost function is used to minimize the error of the control variable. Here, the control variable is the output voltage of the VSI, which decomposed into alpha and beta stationary frames using Clarke's transformation, i.e., $v_{o\alpha}$ and $v_{o\beta}$. The reference signals are also converted into alpha and beta frames, i.e., $v^*_{o\alpha}$ and $v^*_{o\beta}$. The completed equation for the cost function (g_{mpc}) of FCS-MPC can be written as follows:

$$g_{mpc} = |v^*_{o\alpha} - v_{o\alpha}(k+1)| + \left|v^*_{o\beta} - v_{o\beta}(k+1)\right| \tag{31}$$

2.3. Passivity-Based-Model Predictive Control

This section uses a PB-MPC control technique based on the previously designed control techniques. The FCS-MPC control technique and IDA-PBC controllers are merged to form a passivity-based model predictive control technique. Compared with the FCS-MPC control technique, the PB-MPC has the following advantages: (1) Low computational

burden. (2) Free from weighting factors. (3) More robust to parameter mismatch [18]. In the design of the PB-MPC control, the voltage reference signals $v^*_{o\alpha}$ and $v^*_{o\beta}$, defined in the stationary reference frame, are generated by the IDA-PBC controller, and supplied to the cost function of FCS-MPC; they are compared with the predicted voltage vectors in the alpha and beta stationary reference frames of $v_{o\alpha}(k+1)$ and $v_{o\beta}(k+1)$, respectively, as shown in Figure 4.

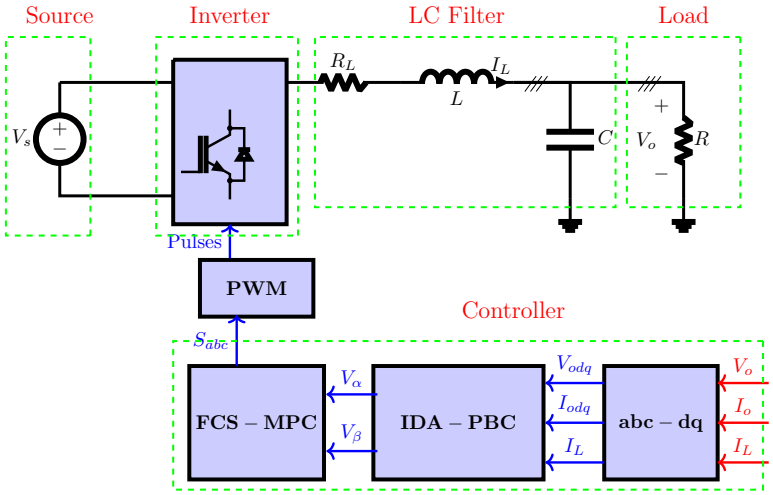

Figure 4. PB-MPC control of the three-phase voltage source inverter with LC filter.

The mathematical model of the PB-MPC control can be derived using IDA-PBC and FCS-MPC predicted equations. So, the complete control technique can be designed using voltage reference equations of IDA-PBC and predicted equations in the cost function of the FCS-MPC. The cost function (g_{pbmpc}) of the PB-MPC control technique can be written as follows:

$$g_{pbmpc} = |v^*_{o\alpha} - v_{o\alpha}(k+1)| + |v^*_{o\beta} - v_{o\beta}(k+1)| \tag{32}$$

3. Simulation Results

This section compares and verifies the performances of the IDA-PBC, FCS-MPC, and PB-MPC controllers using the MATLAB simulation. The three-phase voltage and current waveforms are discussed below for each control technique using three-phase H-bridge inverter topology. The control techniques are compared, based on the type of load supplied individually. The THD performance bar chart is shown at the end of each subsection. The parameters for the VSI are shown in Table 2.

Table 2. Parameters for the three-phase VSI and LC filter.

Parameter	Value	Unit
DC link capacitor voltage V_{dc}	800	V
Fundamental frequency f_g	50	Hz
Switching frequency f_{sw}	10,000	Hz
Filter inductance L	6.5	mH
Resistance of filter inductor R	0.2	Ω
Capacitance of filter C	20	μF

3.1. Performance of Controllers under a Balanced Load

The performances of the IDA-PBC, FCS-MPC, and PB-MPC controllers are investigated using the three-phase VSI under a balanced load in the following subsections.

3.1.1. Performance of the IDA-PBC Controller under a Balanced Load

In linear load conditions, the three-phase voltage and current waveforms for IDA-PBC-controlled VSI are shown in Figure 5.

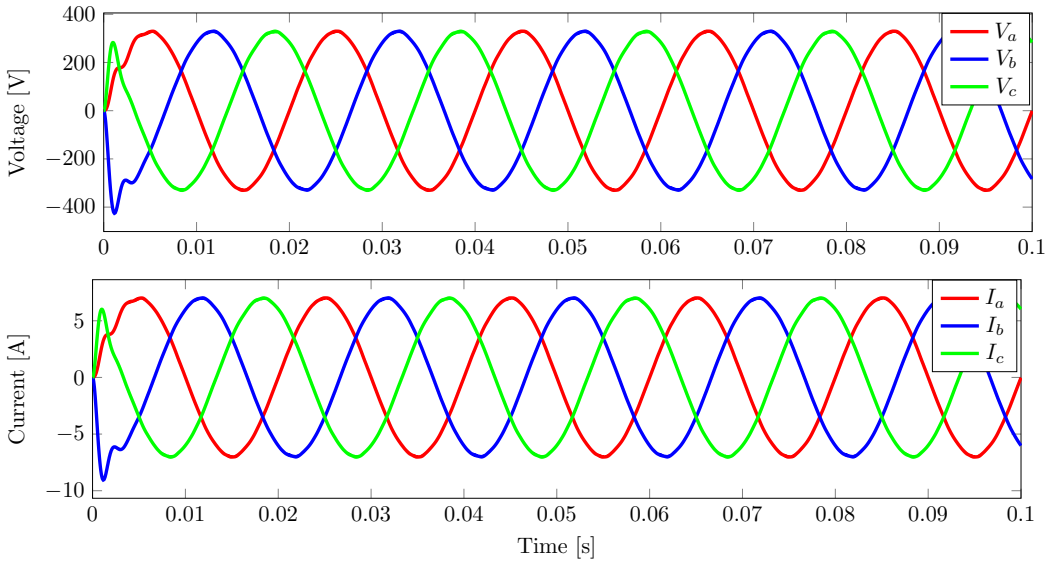

Figure 5. Three-phase voltage and current waveforms of the VSI under a linear load using an IDA-PBC controller.

When a three-phase pure resistive load equal to 23 ohms per phase is connected to the three-phase VSI using an IDA-PBC control technique, its load voltage waveform tracks the reference voltage and can be seen in Figure 5. The IDA-PBC controller controls the output voltage, which tracks the reference voltage with an amplitude equal to 327 V.

Figure 5 also shows the three-phase load current waveforms under a linear resistive load using an IDA-PBC controller for the three-phase VSI. The magnitude and quality of the current depend on the load magnitude, respectively. The THD current value is calculated as 0.39.

3.1.2. Performance of the FCS-MPC Controller under a Balanced Load

The second type of controller is the FCS-MPC controller. The three-phase load voltage waveforms related to the three-phase VSI under a linear balanced load are shown in Figure 6. The inverter's output voltage is the controlled variable, is controlled by FCS-MPC, and is compared with the reference voltage.

The load currents related to the three-phase VSI under a linearly balanced load using an FCS-MPC are shown in Figure 6. The THD value in the current waveform using an FCS-MPC-controlled three-phase VSI under a linear load is 0.75. The three-phase waveforms are sinusoidal and are not distorted as much because of the nature of the load.

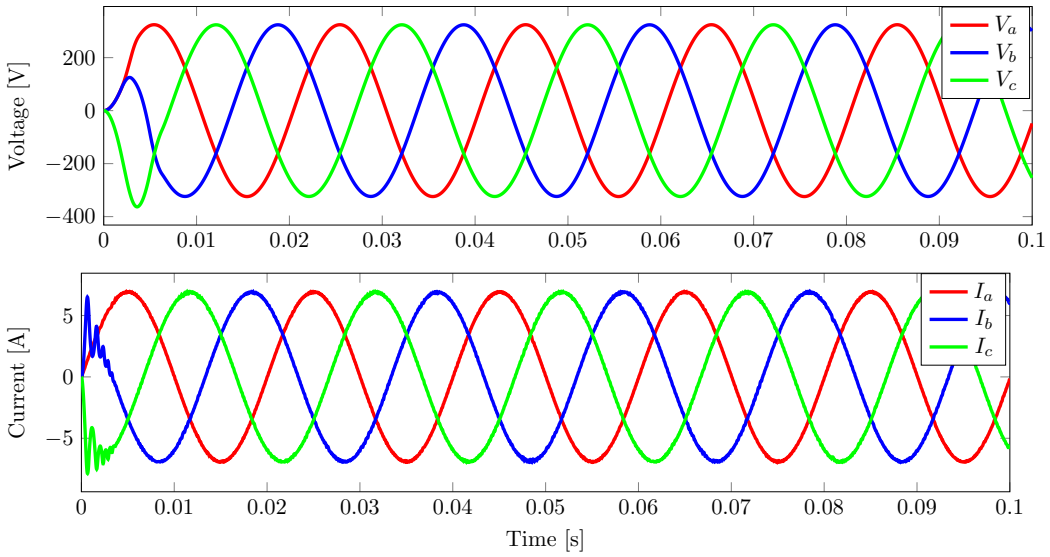

Figure 6. Three-phase voltage and current waveforms of the VSI under a linear load using FCS-MPC controller.

3.1.3. Performance of PB-MPC Controller under a Balanced Load

Under a linear load, the three-phase voltage and current waveforms are shown in Figure 7. The PB-MPC control techniques consist of both IDA-PBC and FCS-MPC control techniques. The IDA-PBC part generates the voltage references, while MPC takes the reference value, measures the controlled variable, and decreases the squared error if there is one. The output current depends on the load; its THD value is 0.39.

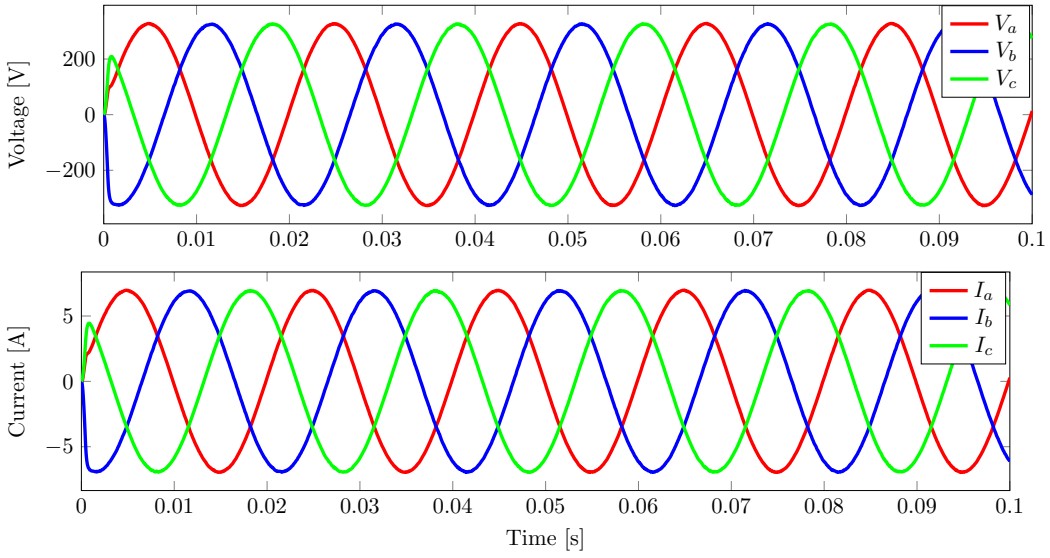

Figure 7. Three-phase voltage and current waveforms of the VSI under a linear load using PB-MPC controller.

At the end of this subsection, the bar chart shows the current THD comparisons for FCS-MPC, IDA-PBC, and PB-MPC controllers during the parameter mismatch in the filter inductor value. As can be seen from Figure 8, under a linear load on the three-phase VSI, the change in the parameters of the filter inductor is also performed; it can be observed that the PB-MPC controller is more robust to the variations of the parameter compared to other controllers and that, comparatively, it has a low current THD. The THD value in the load current can be calculated as follows:

$$THD = \frac{\sqrt{\sum_{k=2}^{\infty}(I_k)^2}}{I_1} \tag{33}$$

Using regression and correlation methods, we calculate the THD value for current waveforms under three different control techniques through the following steps:

Counting sets, calcifying counts, calculating SS_{xy}, and calculating plates a and b.

The numerical values of current THD are plotted in Figure 8.

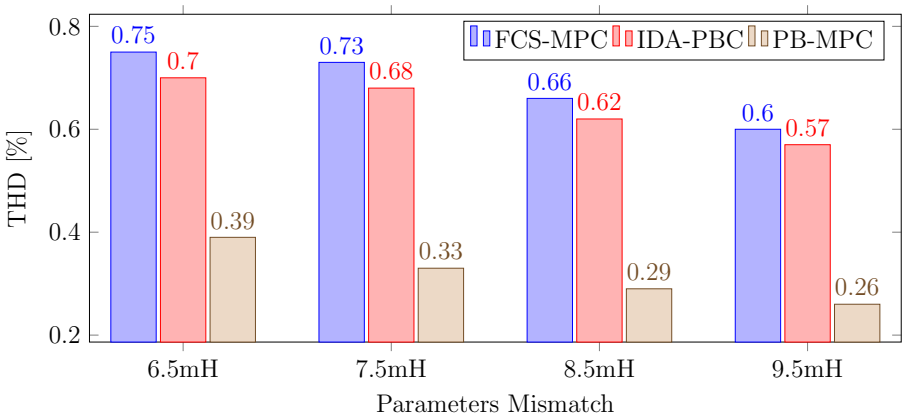

Figure 8. Current THD values using different controllers under a linear load.

3.2. Performances of Controllers under an Unbalanced Load

The performances of the IDA-PBC, FCS-MPC, and PB-MPC controllers are investigated in this subsection using the three-phase VSI under an unbalanced load.

3.2.1. Performance of the IDA-PBC Controller under an Unbalanced Load

Under an unbalanced load, the three-phase voltage and current waveforms are shown in Figure 9. Unbalanced loads of 32 ohms in phase A, 50 ohms in phase B, and 75 ohms in phase C are connected. Despite these unbalanced loads in all phases, the output voltage of the VSI remains constant.

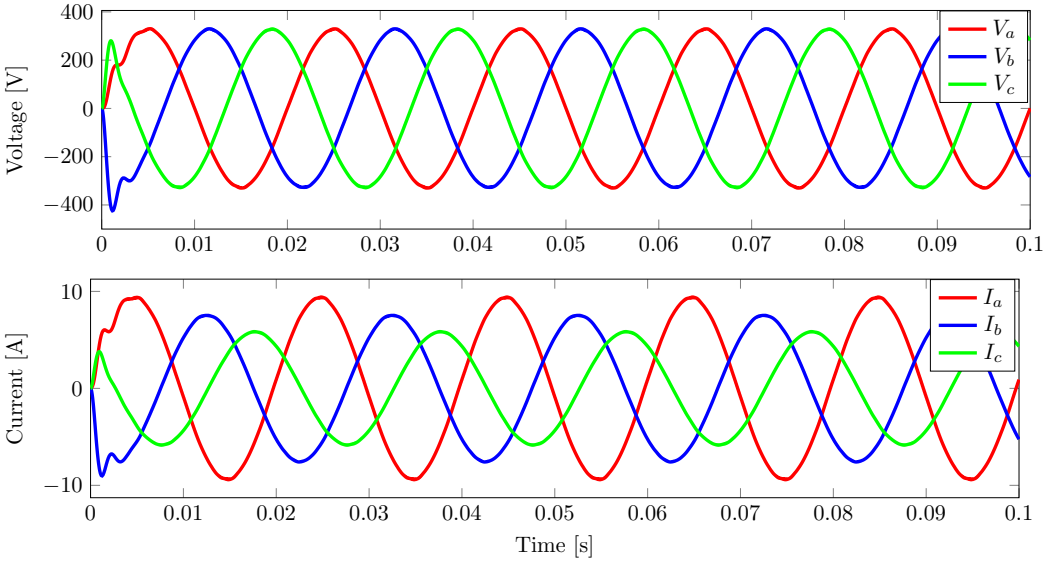

Figure 9. Three-phase voltage and current waveforms of the VSI under an unbalanced load using IDA-PBC controller.

When a three-phase unbalanced load is connected to the three-phase VSI using an IDA-PBC control technique, its load voltage waveform tracks the reference voltage, as can be seen in Figure 9. The three-phase voltage waveform has a peak value of 327 V.

Figure 9 shows the three-phase load current waveforms under an unbalanced load using an IDA-PBC controller for the three-phase VSI. The current amplitude is 10 A in phase A, 6.5 A in phase B, and 4.3 A in phase C.

3.2.2. Performance of the FCS-MPC Controller under an Unbalanced Load

The second type of controller is the FCS-MPC controller. The three-phase load voltage waveforms of the three-phase VSI under an unbalanced load are shown in Figure 10. The unbalanced loads of 32 ohms in phase A, 50 ohms in phase B, and 75 ohms in phase C are connected. Despite these unbalanced loads in all phases, the output voltage of the VSI remains constant.

The load currents of the three-phase VSI under an unbalanced load using an FCS-MPC are shown in Figure 10. The magnitude of the current is 10 A in phase A, 6.5 A in phase B, and 4.3 A in phase C. Compared to the IDA-PBC controller, the FCS-MPC causes a high current THD value and exhibits high distortion at the start of the waveform.

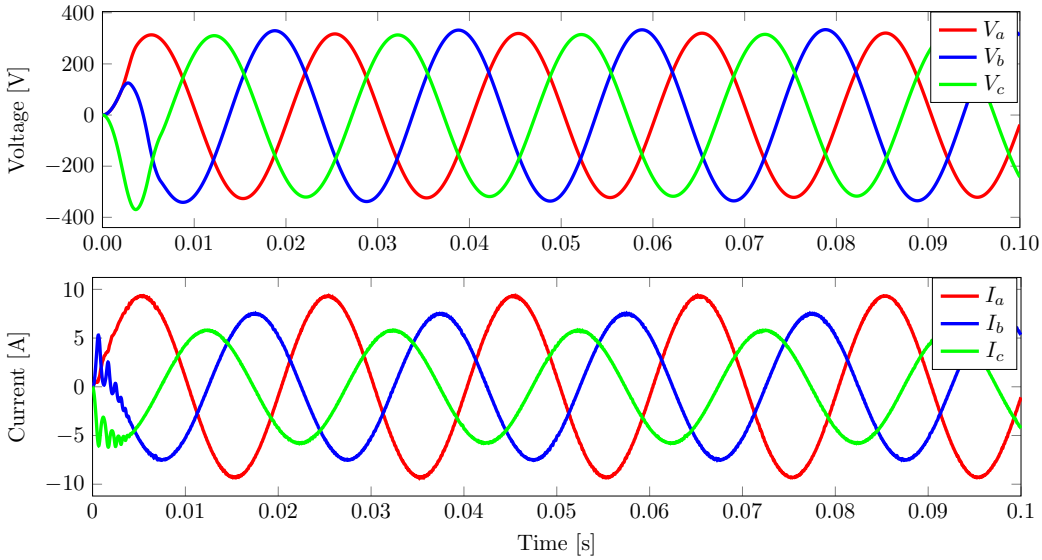

Figure 10. Three-phase voltage and current waveforms of the VSI under an unbalanced load using FCS-MPC controller.

3.2.3. Performance of the PB-MPC Controller under an Unbalanced Load

Under an unbalanced load, the three-phase voltage and current waveforms are shown in Figure 11. The same unbalanced load is connected to the VSI using the PB-MPC controller. The output voltage remains constant, irrespective of the load.

The output currents, using the three-phase VSI, under an unbalanced load and using a PB-MPC controller, have different magnitudes in each phase.

At the end of this subsection, the bar chart shows the current THD comparison for FCS-MPC, IDA-PBC, and PB-MPC controllers under parameter mismatch in the filter inductor value. As can be seen from Figure 12, under an unbalanced load, and with some model changes that occur on the *LC* filter of the three-phase VSI, the PB-MPC controller is more robust in these parameter mismatches in the inductor compared to other controllers and it has a low current THD, comparatively.

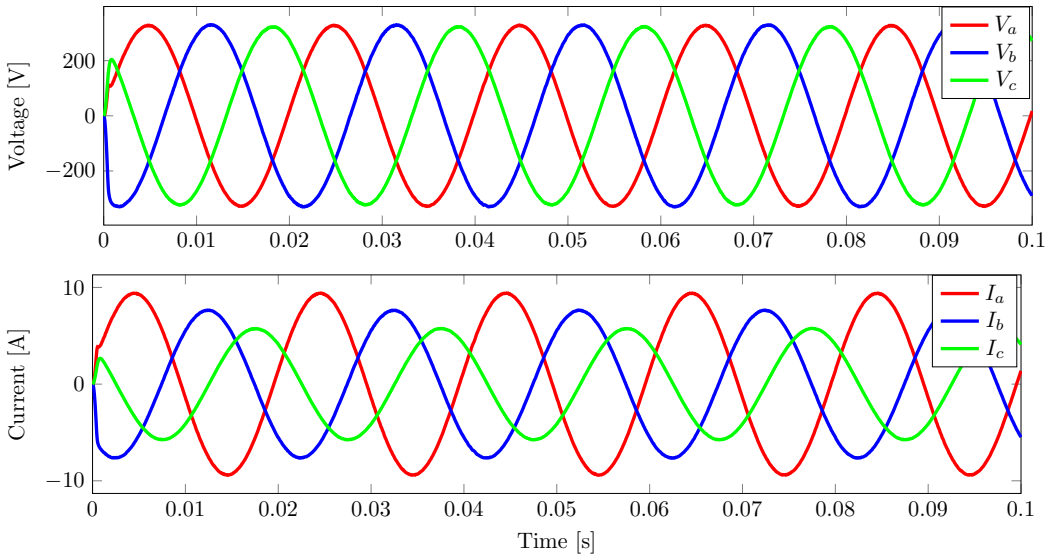

Figure 11. Three-phase voltage and current waveforms of the VSI under an unbalanced load using PB-MPC controller.

Using the regression and correlation method, the THD value is calculated for current waveforms for three different control techniques under an unbalanced load, through these steps:

Counting sets, counting calcified, calculating SS_{xy}, calculating plates a and b.

The numerical values of the current THD are plotted in Figure 12.

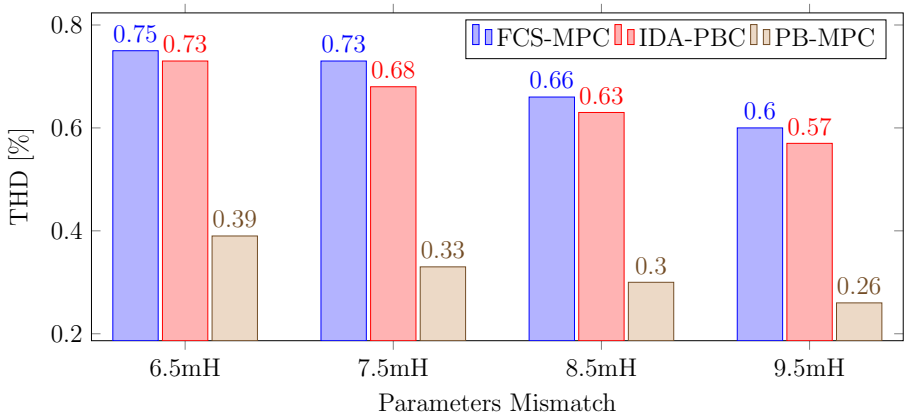

Figure 12. Current THD values of different controllers under an unbalanced load.

3.3. Performances of Controllers under a Non-Linear Load

The performances of the IDA-PBC, FCS-MPC, and PB-MPC controllers are investigated using a three-phase VSI under a non-linear load.

In the non-linear current, short patterns (with periods of 0.033 s) are the harmonics components, which is common in the three-phase rectifier. The main factor affecting these patterns is the AC system's fundamental frequency (i.e., 50 Hz in the current study).

3.3.1. Performance of the IDA-PBC Controller under a Non-Linear Load

Under a non-linear load, the three-phase voltage and current waveforms are shown in Figure 13. Under a non-linear load, the current THD value is 30.33. The output voltage tracks the reference voltage. The three-phase voltage waveforms have a peak value of 327 V.

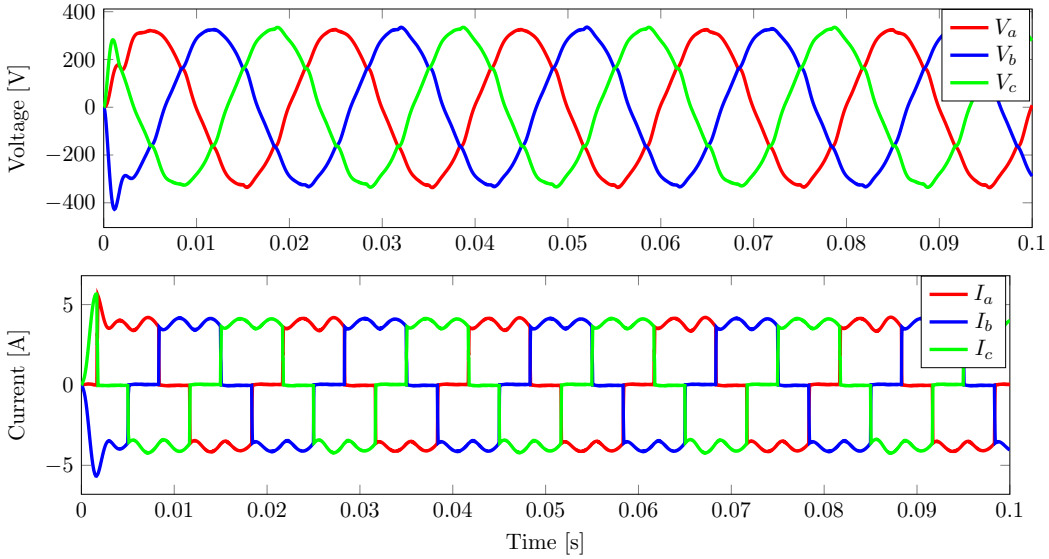

Figure 13. Three-phase voltage and current waveforms of the VSI under a non-linear load using an IDA-PBC controller.

Under a non-linear load, the output currents become distorted and have a high current THD value.

3.3.2. Performance of the FCS-MPC Controller under a Non-Linear Load

The second type of controller is the FCS-MPC controller. The three-phase load voltage waveforms of the three-phase VSI under a non-linear load are shown in Figure 14. As seen from Figure 14, the voltage waveforms have some distortions and high-voltage ripples exist at the start. Moreover, the output voltage tracks the reference voltage after some time.

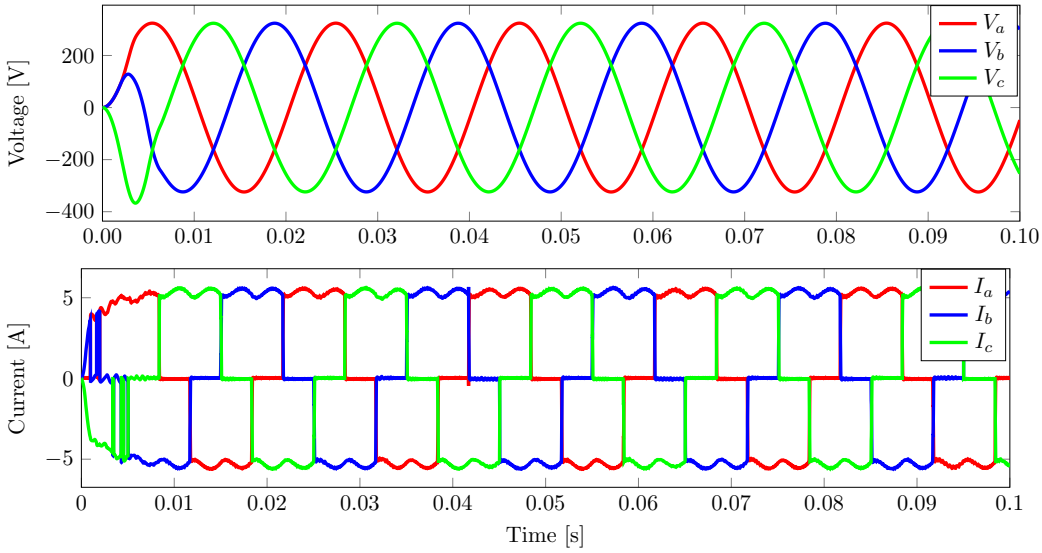

Figure 14. Three-phase voltage and current waveforms of the VSI under a non-linear load using FCS-MPC controller.

The load current of the three-phase VSI under a non-linear load using an FCS-MPC is shown in Figure 14. The output current has high current ripples at the start and a high THD value.

3.3.3. Performance of the PB-MPC Controller under a Non-Linear Load

Under a non-linear load, the three-phase voltage and current waveforms for the PB-MPC-controlled VSI are displayed in Figure 15. During a non-linear load, the output voltage tracks its reference voltage and possesses low voltage ripples at the start, as well as lower THD values compared to the other two control techniques mentioned above.

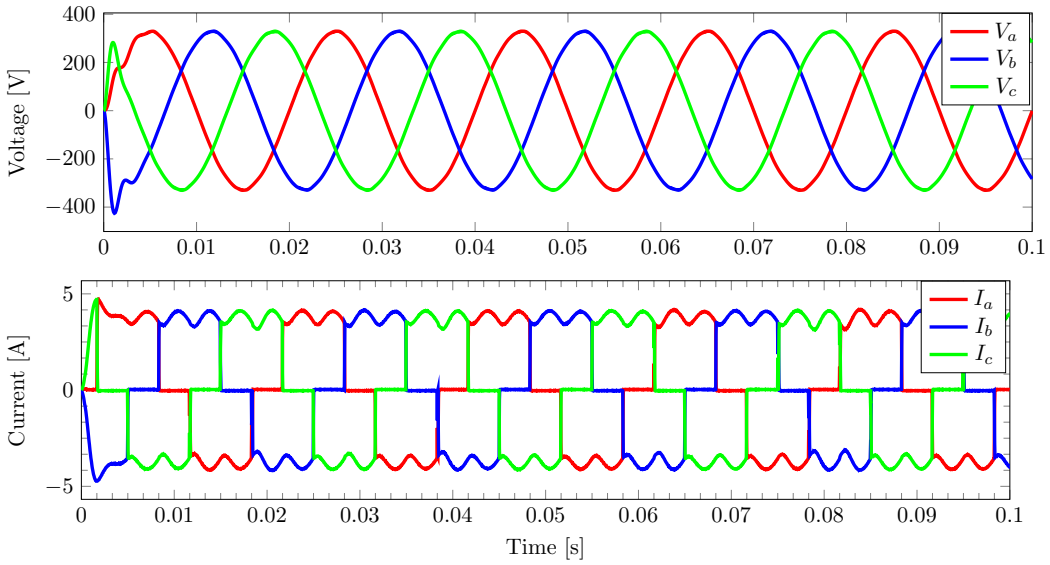

Figure 15. Three-phase voltage and current waveforms of the VSI under a non-linear load using PB-MPC controller.

The non-linear load has $R = 10\ \Omega$ and $C = 4\ uF$. The output currents are shown in Figure 15; it can be seen that there are no high ripples in the output current at the start compared to the other two control techniques.

The bar chart below shows the current THD comparison for FCS-MPC, IDA-PBC, and PB-MPC controllers under a mismatch value in the filter inductance of the LC filter. As seen in Figure 16, the PB-MPC controller is more robust to these parameter variations compared to other controllers and has a comparatively low current THD. The THD value for current waveforms of the three different control techniques is calculated using the regression and correlation method, involving the following steps:

Counting sets, counting calcified, calculating SS_{xy}, calculating plates a and b .

The numerical values of current THD are plotted in Figure 16.

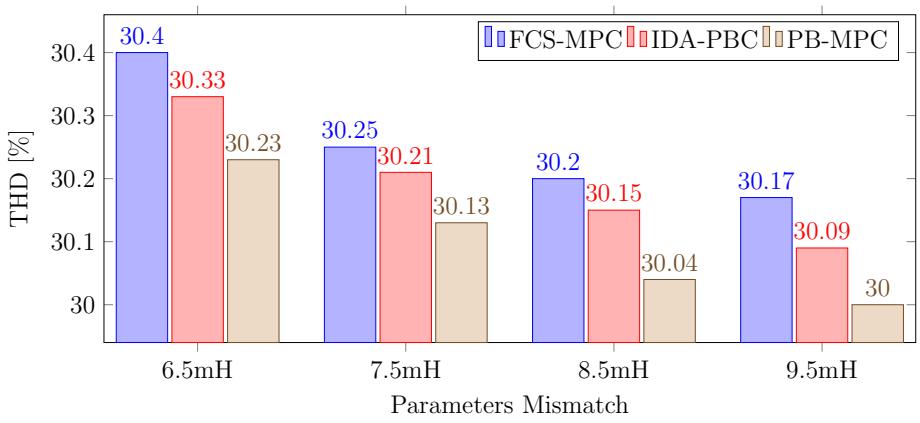

Figure 16. Current THD values of controllers under a non-linear load.

4. Conclusions

This paper has demonstrated through a simulation and numerical results that interconnection damping assignment passivity-based control (IDA-PBC) and passivity-based model predictive control (PB-MPC) are efficient techniques for controlling three-phase voltage source inverters in cases of parameter mismatch and varying load conditions. All the tested controllers operated at a switching frequency of 10 kHz and their performances were evaluated based on this reference switching frequency. The three-phase VSI, utilizing all of the above types of controllers, uses the same control input variables. For instance, the FCS-MPC uses a prediction of control variables, the IDA-PBC measures the system energy and shapes it according to reference signals, and the PB-MPC controller exhibits both characteristics of the FCS-MPC and IDA-PBC controllers. It generates voltage references from the IDA-PBC control part, compares them with the output voltage, and minimizes the error between them (FCS-MPC). It was observed from the simulation results that FCS-MPC has higher current THD values of 0.75%, 0.75%, and 30.4%, the IDA-PBC controller has 0.7%, 0.73%, and 30.3% THD values, while the PB-MPC possesses 0.39%, 0.39%, and 30.23% THD values, under linear, unbalanced, and non-linear loads. It is also clear that, in the case of the PB-MPC controller, THD values did not vary much under mismatch in the filter inductor value and are more robust to the parameter mismatch of the filter inductor than other controllers. In the future, the robustness of the controllers can be extended to the control of parallel connected inverters.

Author Contributions: S.H. designed the system, A.B. and L.V. analyzed the results. M.M. and I.S.M. helped write the paper. All authors have read and agreed to the published version of the manuscript.

Funding: This research received no external funding.

Data Availability Statement: Not applicable.

Conflicts of Interest: The authors declare no conflict of interest.

Abbreviations

The following abbreviations are used in this manuscript:

VSI	voltage source inverter
IDA-PBC	interconnection and damping assignment passivity-based control
FCS-MPC	finite control set model predictive controller
PB-MPC	passivity-based model predictive controller
THD	total harmonic distortion
PWM	pulse width modulation
LC	inductor–capacitor
Fsw	switching frequency
UPS	uninterrupted power supply

References

1. Sonawane, V.R.; Patil, S.B. Track and hunt metaheuristic based deep neural network based fault diagnosis model for the voltage source inverter under varying load conditions. *Adv. Eng. Softw.* **2023**, *177*, 103414. [CrossRef]
2. Rafaq, M.S.; Mohammed, S.A.Q.; Choi, H.H.; Jung, J.W. An improved sliding mode control technique to mitigate mismatched parameter uncertainties of three-phase voltage source inverters. *IEEE Access* **2020**, *8*, 81932–81942. [CrossRef]
3. Lin, B.; Peng, L.; Liu, X. Selective pole placement and cancellation for proportional–resonant control design used in voltage source inverter. *IEEE Trans. Power Electron.* **2022**, *37*, 8921–8934. [CrossRef]
4. Ramezani, M.; Li, S.; Golestan, S. Analysis and controller design for stand-alone VSIs in synchronous reference frame. *IET Power Electron.* **2017**, *10*, 1003–1012. [CrossRef]
5. Hans, F.; Schumacher, W.; Chou, S.F.; Wang, X. Design of multifrequency proportional–resonant current controllers for voltage-source converters. *IEEE Trans. Power Electron.* **2020**, *35*, 13573–13589. [CrossRef]
6. Komurcugil, H.; Altin, N.; Ozdemir, S.; Sefa, I. Lyapunov-function and proportional-resonant-based control strategy for single-phase grid-connected VSI with LCL filter. *IEEE Trans. Ind. Electron.* **2015**, *63*, 2838–2849. [CrossRef]
7. Bao, X.; Zhuo, F.; Tian, Y.; Tan, P. Simplified feedback linearization control of three-phase photovoltaic inverter with an LCL filter. *IEEE Trans. Power Electron.* **2012**, *28*, 2739–2752. [CrossRef]

8. Gupta, R.; Ghosh, A.; Joshi, A. Multiband hysteresis modulation and switching characterization for sliding-mode-controlled cascaded multilevel inverter. *IEEE Trans. Ind. Electron.* **2009**, *57*, 2344–2353. [CrossRef]
9. Zhang, K.; Kang, Y.; Xiong, J.; Chen, J. Direct repetitive control of SPWM inverter for UPS purpose. *IEEE Trans. Power Electron.* **2003**, *18*, 784–792. [CrossRef]
10. Gupta, Y.; Parganiha, N.; Doolla, S. Lyapunov Based Controller for 3ϕ VSI Stage of a UPS and a Distributed Generation Units. In Proceedings of the 2019 10th International Conference on Power Electronics and ECCE Asia (ICPE 2019-ECCE Asia), Busan, Republic of Korea, 27–30 May 2019; pp. 1359–1364.
11. Mohamed, I.S.; Rovetta, S.; Do, T.D.; Dragicević, T.; Diab, A.A.Z. A neural-network-based model predictive control of three-phase inverter with an output *LC* filter. *IEEE Access* **2019**, *7*, 124737–124749. [CrossRef]
12. Mohamed, I.S.; Zaid, S.A.; Abu-Elyazeed, M.; Elsayed, H.M. Classical methods and model predictive control of three-phase inverter with output LC filter for UPS applications. In Proceedings of the 2013 International Conference on Control, Decision and Information Technologies (CoDIT), Hammamet, Tunisia, 6–8 May 2013; pp. 483–488.
13. Riar, B.S.; Scoltock, J.; Madawala, U.K. Model predictive direct slope control for power converters. *IEEE Trans. Power Electron.* **2016**, *32*, 2278–2289. [CrossRef]
14. Dekka, A.; Wu, B.; Yaramasu, V.; Zargari, N.R. Model predictive control with common-mode voltage injection for modular multilevel converter. *IEEE Trans. Power Electron.* **2016**, *32*, 1767–1778. [CrossRef]
15. Shchurov, N.; Myatezh, S.; Malozyomov, B.; Shtang, A.; Martyushev, N.; Klyuev, R.; Dedov, S. Determination of Inactive Powers in a Single-Phase AC Network. *Energies* **2021**, *14*, 4814. [CrossRef]
16. Serra, F.M.; De Angelo, C.H.; Forchetti, D.G. IDA-PBC control of a DC–AC converter for sinusoidal three-phase voltage generation. *Int. J. Electron.* **2017**, *104*, 93–110. [CrossRef]
17. Komurcugil, H. Improved passivity-based control method and its robustness analysis for single-phase uninterruptible power supply inverters. *IET Power Electron.* **2015**, *8*, 1558–1570. [CrossRef]
18. Qiu, L.; Liu, X.; Liu, J.; Ma, J.; Zhang, J.; Li, Y.; Fang, Y. Passivity-Based Cascade-Free Finite-Set Model Predictive Control for Nested Neutral Point-Clamped Converters. *IEEE Access* **2020**, *8*, 200209–200218. [CrossRef]
19. Ojaghi, P.; Rahmani, M. LMI-based robust predictive load frequency control for power systems with communication delays. *IEEE Trans. Power Syst.* **2017**, *32*, 4091–4100. [CrossRef]
20. Ahumada, C.; Cárdenas, R.; Saez, D.; Guerrero, J.M. Secondary control strategies for frequency restoration in islanded microgrids with consideration of communication delays. *IEEE Trans. Smart Grid* **2015**, *7*, 1430–1441. [CrossRef]
21. Wang, J.; Zhang, G.; Wang, R.; Schnelle, S.C.; Wang, J. A gain-scheduling driver assistance trajectory-following algorithm considering different driver steering characteristics. *IEEE Trans. Intell. Transp. Syst.* **2016**, *18*, 1097–1108. [CrossRef]
22. Elbarbary , Z.M.; Hamed, H.A.; El-Kholy, E.E. Comments on "A Performance Investigation of a Four-Switch Three-Phase Inverter-Fed IM Drives at Low Speeds Using Fuzzy Logic and PI Controllers". *IEEE Trans. Power Electron.* **2022**, *33*, 8187–8188. [CrossRef]
23. Ortega, R.; Van Der Schaft, A.; Maschke, B.; Escobar, G. Interconnection and damping assignment passivity-based control of port-controlled Hamiltonian systems. *Automatica* **2002**, *38*, 585–596. [CrossRef]
24. Ortega, R.; Van Der Schaft, A.J.; Mareels, I.; Maschke, B. Putting energy back in control. *IEEE Control. Syst. Mag.* **2001**, *21*, 18–33.
25. Gupta, Y.; Chatterjee, K.; Doolla, S. Controller design, analysis and testing of a three-phase VSI using IDA–PBC approach. *IET Power Electron.* **2020**, *13*, 346–355. [CrossRef]
26. Cortés, P.; Ortiz, G.; Yuz, J.I.; Rodríguez, J.; Vazquez, S.; Franquelo, L.G. Model predictive control of an inverter with output *LC* filter for UPS applications. *IEEE Trans. Ind. Electron.* **2009**, *56*, 1875–1883. [CrossRef]
27. Albalawi, H.; Bakeer, A.; Zaid, S.A.; Aggoune, E.H.; Ayaz, M.; Bensenouci, A.; Eisa, A. Fractional-Order Model-Free Predictive Control for Voltage Source Inverters. *Fractal Fract.* **2023**, *7*, 433. [CrossRef]
28. Bakeer, A.; Mohamed, I.S.; Malidarreh, P.B.; Hattabi, I.; Liu, L. An Artificial Neural Network-Based Model Predictive Control for Three-Phase Flying Capacitor Multilevel Inverter. *IEEE Access* **2022**, *10*, 70305–70316. [CrossRef]